DOI: 10.1002/chem.201001294

Photophysical Studies of Dipolar Organic Dyes That Feature a 1,3-Cyclohexadiene Conjugated Linkage: The Implication of a Twisted Intramolecular Charge-Transfer State on the Efficiency of Dye-Sensitized Solar Cells

Kuan-Fu Chen,[a, b] Che-Wei Chang,[a] Ju-Ling Lin,[a] Ying-Chan Hsu,[a] Ming-Chang P. Yeh,*[b] Chao-Ping Hsu,*[a] and Shih-Sheng Sun*[a]

Abstract: A detailed study of the synthesis and photophysical properties of a new series of dipolar organic photosensitizers that feature a 1,3-cyclohexadiene moiety integrated into the π-conjugated structural backbone has been carried out. Dye-sensitized solar cells (DSSCs) based on these structurally simple dyes have shown appreciable photo-to-electrical energy conversion efficiency, with the highest one up to 4.03%. Solvent-dependent fluorescence studies along with the observation of dual emission on dye **4b** and single emission on dyes **4a** and **32** suggest that dye **4b** possesses a highly polar emissive excited state located at a lower-energy position than at the normal emissive excited state. A detailed photophysical investigation in conjunction with computational studies confirmed the twisted intramolecular charge-transfer (TICT) state to be the lowest emissive excited state for dye **4b** in polar solvents. The relaxation from higher-charge-injection excited states to the lowest TICT state renders the back-electron transfer process a forbidden one and significantly retards the charge recombination to boost the photocurrent. The electrochemical impedance under illumination and transient photovoltage decay studies showed smaller charge resistance and longer electron lifetime in **4b**-based DSSC compared to the DSSCs with reference dyes **4a** and **32**, which further illustrates the positive influence of the TICT state on the performance of DSSCs.

Keywords: charge transfer · cyclohexadiene · density functional calculations · dyes/pigments · photochemistry

Introduction

The search for clean and alternative energy has become an important and difficult issue in the 21st century. Among several new energy technologies, solar energy seems to be one important answer to this question. Dye-sensitized solar cells (DSSCs) based on organic and coordination complexes have received great attention since the seminal report by Grätzel and co-workers in 1991.[1] Ru^{II}-based complexes such as N3, N719, black dye, and others have shown the best photoconversion efficiency—up to approximately 11%—under air mass (AM) 1.5 irradiation thus far.[2] Although the efficiency of DSSCs based on organic dyes are generally lower than the cells based on Ru^{II} dyes, the highest photoconversion efficiency of organic dye-sensitized solar cells has exceeded 9%.[3] The advantages of organic dyes over Ru^{II}-based metal complexes in DSSCs include the typically high molar absorption coefficients of organic dyes ($\varepsilon > 20000\,M^{-1}cm^{-1}$), a variety of specific functional groups of organic dyes available for tuning the absorption spectra coverage, the relatively low costs of organic dye compared with those of ruthenium-based metal complexes, and essentially no limitation of resources.[4]

The generation of photocurrents in a DSSC occurs through the following processes.[5] First, the dye sensitizer

[a] K.-F. Chen, C.-W. Chang, J.-L. Lin, Dr. Y.-C. Hsu, Dr. C.-P. Hsu, Dr. S.-S. Sun
Institute of Chemistry, Academia Sinica (Taiwan, ROC)
Fax: (+886) 2-2783-1237
E-mail: cherri@chem.sinica.edu.tw
sssun@chem.sinica.edu.tw

[b] K.-F. Chen, Prof. M.-C. P. Yeh
Department of Chemistry
National Taiwan Normal University (Taiwan, ROC)
Fax: (+886) 2-2932-4249
E-mail: cheyeh@ntnu.edu.tw

Supporting information for this article is available on the WWW under http://dx.doi.org/10.1002/chem.201001294.

absorbs a photon (sunlight) to generate the photoexcited state of the dye (S*). Next, the photoexcited dye (S*) injects an electron into the conduction band (CB; −0.5 V versus the normal hydrogen electrode (NHE)) of TiO_2. The resulting oxidized dye is subsequently reduced back to its original state by electron donation from the redox mediator (I^-/I_3^-) in the electrolyte solution. The injected electrons move through the network of interconnected TiO_2 nanoparticles to arrive at the transparent conducting oxide (fluorine-doped tin oxide, FTO) and then through the external circuit to the counter-electrode (Pt-coated glass). The I^- ion is regenerated by the reduction of the triiodide ion (I_3^-) at the counterelectrode through the donation of electrons from the external circuit. Then the circuit is completed. During this electron-flow cycle, there are undesirable side processes: the electrons injected into the CB of the TiO_2 electrode may recombine either with oxidized dye, or with I_3^- at the TiO_2 surface, thus resulting in lower photovoltaic performances of the DSSCs.

Thus, one of the key issues to enhance the performance of a DSSC is how efficient the system is able to shuffle the hole generated from a photoexcited dye away from the TiO_2 surface to prevent the undesirable charge-recombination processes. The electron density of the HOMOs in thiocyanate-substituted Ru^{II} dyes is typically spread over the Ru^{II} center and NCS ligands, which reduces the probability of charge recombination.[6] A similar strategy of integration of electron-rich moieties such as thiophene or furan in the ancillary ligand in Ru^{II} complexes or metal free dyes also partially delocalizes the HOMO electron density distribution away from TiO_2 surface.[7] Organic dyes with a structural framework that features a D–D–π–A arrangement have been designed for creating charge-transfer cascades to enhance charge separation.[8] Incorporation of secondary electron-transfer cascades within the dye structure to increase the separation between the oxidized dye and the TiO_2 surface is also capable of effectively retarding the charge-recombination kinetics and produces a long-lived charge-separated state.[9] On the other hand, an excited-state conformational distortion after charge injection to render the charge recombination a forbidden process would be an ideal alternative to slow down the charge-recombination kinetics between the injected electron and the oxidized dye.

Photoinduced intramolecular charge transfer (ICT) in a strong electron donor–acceptor-substituted conjugated system normally displays a prominent solvatochromic effect.[10] In a nonpolar solvent, the locally excited (LE) state takes a planar conformation and the excited state is stabilized with increasing solvent polarity. In some extreme cases, the donor and acceptor fragments are twisted and the excited molecule is further relaxed to a twisted intramolecular charge-transfer (TICT) state in polar solvents.[11] The representative example with such low-lying TICT state in polar solvents is *N*,*N*-dimethylaminobenzonitrile (DMABN), in which twisting about the benzonitrilo–dimethylamino C–N bond in the LE state has been proposed to be responsible for the observed dual emission.[11] The formation of a TICT state would generate a significant charge separation between the donor–acceptor pair and thus a large dipole moment in the excited state. A notable characteristic of the TICT state is its nearly electronically decoupled donor–acceptor pair with forbidden radiative transition from the TICT state to the ground state. We envision that an organic dye with a strong electronically coupled dipolar donor–acceptor bridged by a suitable π-conjugated spacer with an accessible low-lying TICT state could be advantageous for DSSCs. The relaxation from the Franck–Condon state to the TICT state upon photoexcitation of the dipolar dye followed by charge injection into the TiO_2 conduction band would enhance the photocurrent due to the forbidden nature of charge recombination between the injected electron and the oxidized dye.

Previously, we have reported a series of structurally simple dipolar organic dyes that feature a cyclohexadiene moiety in the conjugation framework.[12] The DSSCs assembled based on these dyes showed appreciable efficiency of up to 4.0% relative to the 5.8% of N719 dye efficiency under the same experimental conditions. The relatively good performance of these dyes is partially ascribed to the compact structures that increased the dye loading onto the TiO_2 surface and compensated for the narrow spectral coverage of light harvesting. The comparable dye loading and absorption spectral coverage between dyes **4a** and **4b** would lead to the expectation of similar light-harvesting ability and photocurrent density generated between these two dyes. However, the incident photon-to-current efficiency (IPCE) value at absorption maxima and photocurrent density of the **4a**-based device are almost 20% less than the **4b**-based device. Herein, we report the photophysical studies, electrochemical impedance spectroscopy, and transient photovoltage measurements for dyes **4a**, **4b**, and model compound **32** to elucidate the possible TICT mechanism and its implication on the efficiency of DSSCs. The results have clearly shown that the TICT state in dye **4b** plays an important role in the photocurrent process.

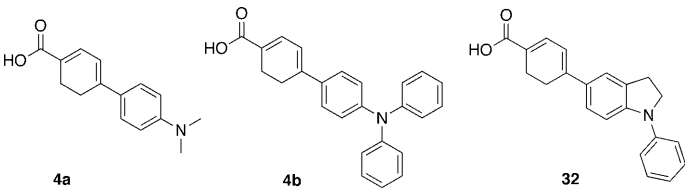

4a **4b** **32**

Results and Discussion

Synthesis of the materials: The synthesis of **4a** and **4b** has been reported previously.[12] Scheme 1 describes the synthesis of dye **32**. This molecule was designed to serve as a model compound by fusing the benzene phenylamino moiety to prevent the twisting of the C–N bond in the excited states to assess the accessibility of the TICT state in **4a** and **4b**. The key intermediate, 5-bromo-1-phenylindoline,

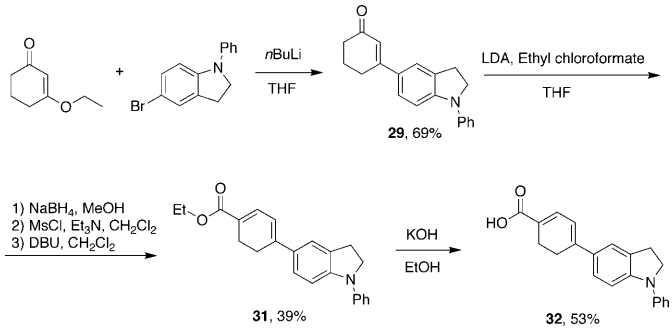

Scheme 1. Synthesis of dye **32**.

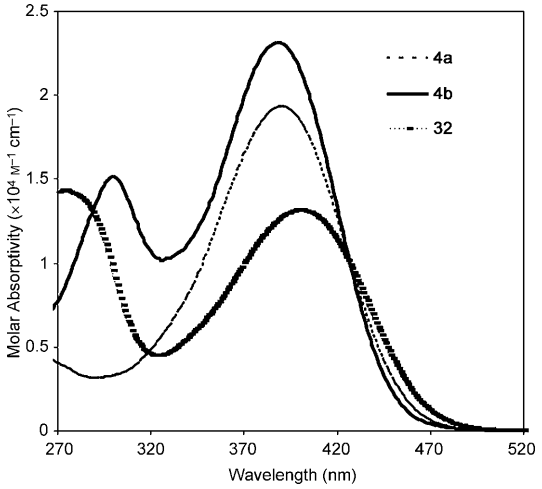

Figure 1. Electronic absorption spectra of **4a**, **4b**, and **32** in acetonitrile.

was prepared by palladium-catalyzed Buchwald–Hartwig C–N coupling reaction of 5-bromoindoline with 1-iodobenzene according to the published methods.[13] All three dyes with 1,3-cyclohexadiene in the structural framework exhibit fairly good thermal stability and show no decomposition up to 200 °C as evidenced by the thermogravimetric analysis (TGA) data.

Electronic absorption spectra: The absorption spectra in acetonitrile for the three dyes are shown in Figure 1. The related photophysical data are summarized in Table 1. The general features of the absorption spectra consist of one broad band in the visible region and a less intense absorption band in the near-UV region, which correspond to the ICT transition and the locally excited π–π* transition, respectively.[12] The absorption spectra for all three dyes vary little with a difference of only a few nanometers with respect to the solvent polarity, thus suggesting a small difference in dipole moments between the ground state and Franck–Condon excited state. The slightly more redshifted ICT band in dye **32** than the ICT bands in dyes **4a** and **4b** is in accordance with the more planar geometry in **32** due to the structural fixation of the C–N bond rotation.

Table 1. Absorption (λ_{abs}) and fluorescence (λ_{em})[a] maxima, Stokes shifts ($\Delta\nu_{st}$),[b] fluorescence quantum yields (Φ_f), lifetimes (τ), and radiative (k_r) and nonradiative (k_{nr}) rate constants for dyes **4a**, **4b**, and **32** in different solvents.

Dye	Solvent	λ_{abs} [nm]	λ_{em} [nm]	$\Delta\nu_{st}$ [cm^{-1}]	Φ_f	τ [ns]	k_r [10^8 s^{-1}]	k_{nr} [10^8 s^{-1}]
4a	diethyl ether	380	406	1685	0.11	1.5	0.72	5.82
	toluene	400	413	787	0.14	1.5	0.93	5.79
	THF	385	430	2718	0.20	1.6	1.21	4.92
	MeCN	392	481	4720	0.08	2.5	0.32	3.72
4b	diethyl ether	398	434	2084	0.11	1.8	0.60	4.93
	toluene	400	435	2011	0.12	1.7	0.66	5.09
	THF	384	458	4208	0.14	1.7	0.80	4.98
	MeCN	389	530	6839	0.03	2.2,[c] 3.6[d]	0.08[e]	2.75[e]
32	diethyl ether	391	423	1935	0.07	1.6	0.44	5.97
	toluene	411	430	1075	0.14	1.7	0.84	4.98
	THF	395	448	2995	0.10	1.7	0.58	5.20
	MeCN	399	496	4902	0.08	2.6	0.31	3.57

[a] Fluorescence data are from corrected spectra. [b] $\Delta\nu_{st}=\nu_{abs}-\nu_{em}$. [c] Fitted lifetime monitored at a wavelength of 450 nm. [d] Fitted lifetime monitored at a wavelength of 600 nm. [e] The values were calculated based on the quantum yield of the whole emission profile and lifetime value of 3.6 ns.

Fluorescence properties and solvatochromic effect: The fluorescence quantum yields, excited-state lifetimes, and calculated radiative and nonradiative rate constants for dyes **4a**, **4b**, and **32** in diethyl ether, toluene, THF, and acetonitrile at room temperature were collected in Table 1. In contrast to the minor solvent-dependent absorption spectral features, the fluorescence spectra of **4a**, **4b**, and **32** vary significantly with increasing solvent polarity, which is indicative of a pronounced charge-transfer nature of the emissive states. Both **4a** and **32** exhibit a monotonic redshift of fluorescence maximum upon increasing solvent polarity. The emission maxima of bathochromic **4a** shift from 406 nm in diethyl ether to 481 nm in acetonitrile, whereas the emission maxima of bathochromic **32** shift from 423 nm in diethyl ether to 496 nm in acetonitrile. The emission is apparently dominated by ICT for both **4a** and **32**. The related photophysical parameters including quantum yields and excited-state lifetimes for these two dyes are also comparable.

The emission of **4b** showed even more prominent bathochromic shift than **4a** and **32** with increasing solvent polarity, which indicates a larger dipole moment for the emissive state of **4b** than **4a** and **32** (see Figure 2). It is consistent with the order of the obtained excited-state dipole moments (μ_e) in which the μ_e values follow an order of **4a** < **32** < **4b** (vide infra). However, unlike the cases of **4a** and **32** in which the excited-state decay in acetonitrile showed single exponential process, the excited-state decay of **4b** in acetonitrile displayed a biexponential process with fitted lifetime values of 2.2 and 3.6 ns for monitoring the emission profile

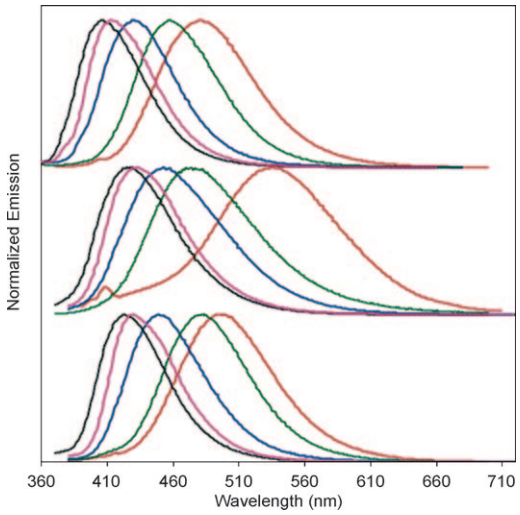

Figure 2. Normalized fluorescence spectra of **4a** (top), **4b** (middel), and **32** (bottom) in diethyl ether (black curve), toluene (pink curve), THF (blue curve), CH_2Cl_2 (green curve), and acetonitrile (red curve).

at 450 and 600 nm, respectively. The same excitation-spectral profiles observed when monitoring at these two wavelengths indicate that the two excited states under equilibrium originate from the same ground-state species.[14]

The solvatochromic properties of the three dyes were further examined by Lippert–Mataga analysis (Figure S1 in the Supporting Information).[15] The excited-state dipole moment (μ_e) can be extracted from the slope of the solvatochromic plot (m_f) of the Stokes shift (ν_{st}) against the solvent parameter Δf according to Equations (1–3):

$$\Delta\nu_{st} = -[(^1/_4\pi\varepsilon_0)(2/hca^3)][\mu_e(\mu_e-\mu_g)]\Delta f + \text{constant} \quad (1)$$

$$\Delta f = (\varepsilon-1)/(2\varepsilon+1) - 0.5(n^2-1)/(2n^2+1) \quad (2)$$

$$a = (3M/4N\pi d)^{1/3} \quad (3)$$

in which μ_g is the ground-state dipole moment, ε is the solvent dielectric constant, ε_0 is the vacuum permittivity, n is the solvent refractive index, h is the Planck constant, c is the velocity of light, and a is the Onsager radius of solute, which can be derived from the Avogadro number N, molecular weight M, and density d. The value of μ_g was calculated using density functional theory with the B3LYP/6-31G* basis set. The obtained dipole moments of the emissive excited state and related parameters are summarized in Table 2. Indeed, the obtained emissive excited-state dipole moments of **4b** from Lippert–Mataga analysis is larger than the corresponding emissive excited-state dipole moments of **4a** and **32**. With a large emissive excited-state dipole moment for **4b** and comparable excited-state dipole moments for **4a** and C–N-bond-fused **32**, it may be possible for the emissive excited state of **4b** in polar solvents to originate from a TICT state.

Table 2. Ground- and excited-state dipole moments for **4a**, **4b**, and **32**.

Dye	a [Å][a]	m_f [cm^{-1}][b]	μ_g [D][c]	μ_e [D]
4a	4.66	9409	5.97	13.18
4b	5.35	16457	3.48	17.77
32	5.1	8465	4.04	12.79

[a] Onsager radius calculated by Equation (3) with $d = 1.0\ g\,cm^{-3}$ for **4a**, **4b**, and **32**. [b] Calculated on the basis of Equation (1). [c] Calculations at the B3LYP/6-31G* level.

In general, a TICT state is likely to form with a strong electron donor–acceptor pair linked with a short π-conjugated framework in a polar medium in which the electron density of the charge-separated species is nearly localized on the donor–acceptor ends. Han et al. have reported a thiophene π-conjugated donor–acceptor system with emission that originates from a low-lying TICT state in polar solvents.[11n] Tang and co-workers also reported a series of diphenylamine boron dipyrromethene dipolar π-conjugated molecules that show emission from TICT in highly polar solvents.[11m] A series of aminostilbenes reported by Yang et al. has been demonstrated to possess an accessible TICT state, and the molecules are able to relax to the TICT state upon photoexcitation in polar solvents by twisting the corresponding C–N bond.[11b,o] In our current studies, when the C–N bond is fused to restrict the rotation around the benzene diphenylamino C–N bond as in the case of **32**, essentially all the photophysical parameters for **32** are similar to **4a** in which typical ICT properties were observed. The radiative rate constant of **4b** in acetonitrile is four times smaller than the corresponding values for **4a** and **32**. It should be noted here that the calculated radiative rate constant for **4b** was based on the quantum yield of a full emission profile in which two emissive states are under equilibrium, and thus the obtained k_r value represents only an upper limit for the radiative rate constant. These results suggest that a less-permitted radiative transition from the emissive state to the ground state exists in **4b** when compared to the excited-state deactivation pathways of **4a** and **32**. The emissive states of **4b** in acetonitrile, therefore, are tentatively assigned to a higher-energy ICT state with a lifetime of 2.2 ns and a lower-energy TICT state with a lifetime of 3.6 ns. Upon relaxation from the Franck–Condon state, polar acetonitrile can effectively stabilize the ICT state, which is followed by further geometric twisting of the C–N bond to relax to a TICT state.

The torsional barriers for the deactivation process from an ICT state to a TICT state were evaluated by temperature-dependent fluorescence in acetonitrile and DMSO. Assuming such torsional motion is the only activated singlet-decay process and the intersystem crossing is negligible, the activation energy, E_a, for the torsional motion can be estimated from Equation (4):[16]

$$\ln(\Phi_f^{-1}-1) = \ln(A_0/k_r) - E_a/RT \quad (4)$$

in which Φ_f is the fluorescence quantum yield measured at temperature T, and A_0 is the Arrhenius constant. An Arrhenius plot of $\ln(\Phi_f^{-1}-1)$ against $1/T$ will give an E_a value for

the torsional motion. Figure 3 illustrates the Arrhenius plots of **4b** in acetonitrile and DMSO. The calculated torsional barriers for **4b** in acetonitrile and DMSO are 1.1 and

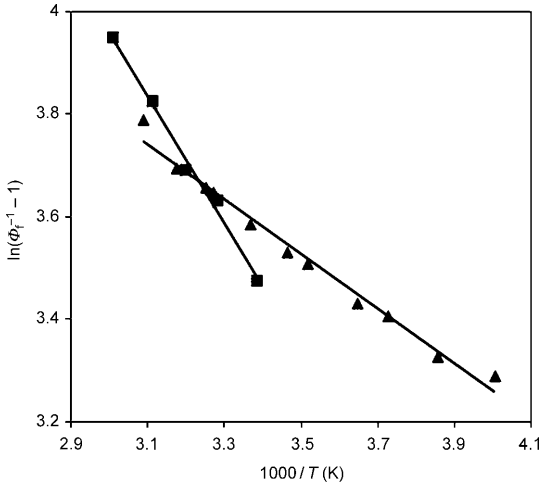

Figure 3. Arrhenius plots of **4b** in acetonitrile (▲) and DMSO (■).

2.4 kcal mol^{-1}, respectively. The small activation barriers for the torsional motion of **4b** in polar solvents indicate a facile conversion from an ICT state to a relaxed TICT state. It is interesting to note that there is a small difference in the torsional barriers in acetonitrile and DMSO. This difference can be attributed to the more viscous DMSO relative to acetonitrile, which leads to a higher activation energy for the conformational rearrangement in DMSO. Assuming k_r is temperature-independent in the experimental temperature range, the pre-exponential A_0 values in acetonitrile and DMSO are 1.7×10^9 and 2.7×10^{10} s^{-1}, respectively, which are smaller than the values for typical gas-phase unimolecular reactions (10^{12}–10^{14} s^{-1}), thereby indicating a strong solvation effect in these polar solvents during the torsional motion to yield a more organized activated complex than the pretwisted conformation and result in a negative entropy of activation.

Computational approach: To further support the existence of an accessible TICT state in **4b**, detailed quantum calculations were carried out for **4a**, **4b**, and **32**. The molecular structures of ground and electronically excited states of all three compounds in planar and twisted conformations were optimized. The frontier molecular orbitals (MOs) and electronic transitions were calculated with DFT and time-dependent (TD)-DFT at the B3LYP/6-31G* level; results are summarized in Table 3 and Figure 4. The S_1 state of all three compounds corresponds to a HOMO→LUMO transition, whereas the S_2 state corresponds to either HOMO−1→LUMO or HOMO→LUMO+1. In Figure 5 it can clearly be seen that the frontier MOs are more localized in twisted conformations than in planar structures. The electron density of the HOMO is localized on the donor moiety, whereas

Table 3. Calculated vertical electronic transitions for all compounds in planar and twisted conformations.

Dye	Conformation	State	λ_{abs} [nm]	f	Excitation[a]	%
4a	planar	S_1	398	0.7853	H→L	100
		S_2	300	0.057	H−1→L	92
					H→L+2	6
	twisted	S_1	439	0.0003	H→L	97
		S_2	352	0.7088	H−1→L	100
4b	planar	S_1	410	0.8833	H→L	99
		S_2	330	0.0339	H→L+1	96
	twisted	S_1	465	0.1300	H→L	98
		S_2	349	0.7041	H−1→L	100
32	planar	S_1	450	0.0548	H→L	98
		S_2	350	0.6589	H−1→L	97

[a] H and L represent HOMO and LUMO, respectively.

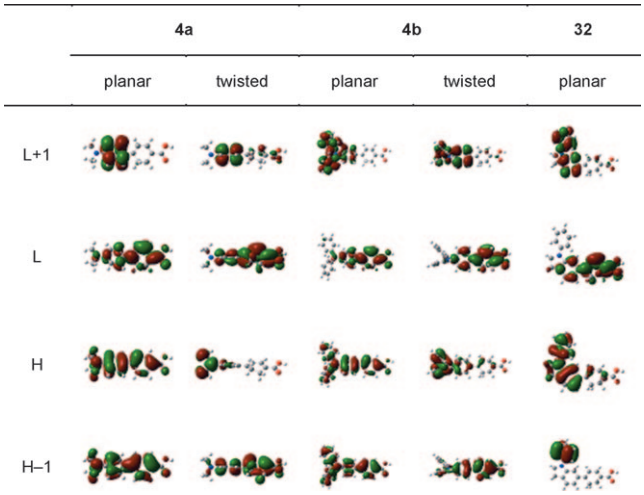

Figure 4. Frontier molecular orbitals for **4a**, **4b**, and **32** in planar and twisted conformations.

the LUMO is localized on the acceptor moiety for the perpendicular conformation. Thus, a more prominent charge separation exists in the perpendicular conformation than the planar conformation.

Potential-energy curves as a function of the twisting angle between the C–N bond were calculated for the ground and low-lying excited states of **4a** and **4b** with TD-DFT at the B3LYP/6-31G* level. The results are depicted in Figure 5. Unlike the case of **4a**, in which the lowest-energy conformations in both S_0 and S_1 states are planar, the conformation of **4b** reaches a low-energy plateau in the S_1 state with twisted angle between 70 and 90°. Based on the potential-energy curve of **4b**, the S_1 state at the twisted conformation is approximately 0.28 eV lower in energy than the planar conformation. It should be noted here that the conformation of **4b** in the TICT state is not necessarily twisted at 90° along the C–N bond, which is slightly different from the conventional definition of the TICT state. The potential-energy curve of the ground state has a minimum of 32° twisted geometry for **4b**. The partial pretwisted C–N bond of **4b** in the ground state ensures that there is less energy required to overcome the rotation barrier to cross the potential surface from the

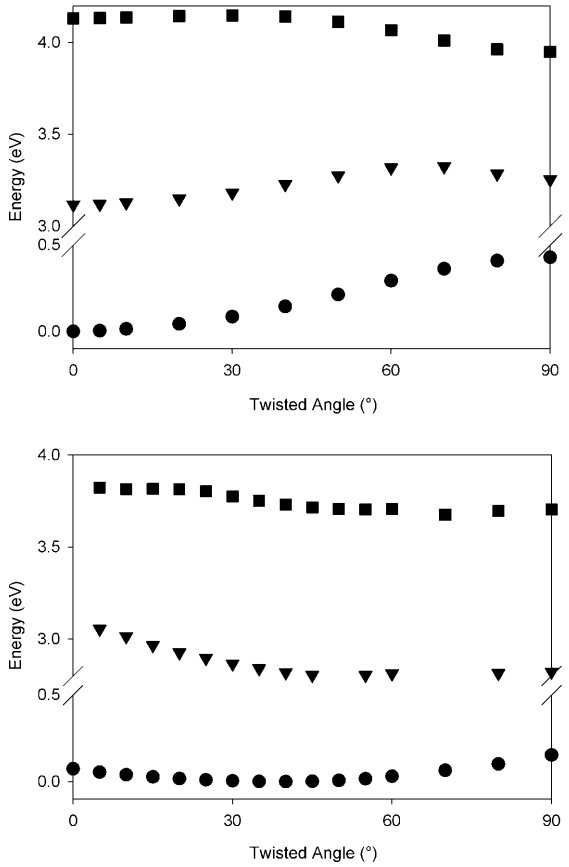

Figure 5. Calculated potential-energy curves as a function of twisting angle for different electronic states for **4a** (top) and **4b** (bottom) with TD-DFT at the B3LYP/6-31G* level (●=S0, ▼=S1, and ■=S2).

planar ICT state to the lowest-energy TICT state when compared to the relaxation process in **4a**.

Properties of DSSCs assembled based on dyes 4a, 4b, and 32: The amount of dye loading and the electrochemical data of DSSCs assembled based on dyes **4a**, **4b**, and **32** are collected in Table 4. Figure 6 shows the absorption spectra of the three dyes adsorbed on a transparent TiO_2 film. Compared to the corresponding spectra in acetonitrile solution, the absorption spectral coverage of the dyes becomes broader upon adsorption on TiO_2, but the absorption maxima shifted to higher energy when compared to that of in solution. Such a blueshift of the absorption spectra is attributed to either the formation of H-type aggregate[17] or deprotonation of the carboxylic acid.[7c] The spectral coverage of **4b** is apparently broader than the ones of **4a** and **32**, which implies potentially better light harvesting for **4b**. The amount of dyes adsorbed on the TiO_2 surface was estimated from the difference in concentration of each solution before and after TiO_2 film immersion followed by rinsing with acetonitrile to ensure a minimum of the physically adsorbed dyes left on the films. The amount of dye adsorbed onto the TiO_2 film is extremely large, most likely due to the compact molecular size of dyes.[18] The high dye loading on the TiO_2 film indicates that these structurally simple dyes with small molecular sizes formed a well-organized monolayer on the TiO_2 surface, which is beneficial for light-harvesting efficiency.[19]

Table 4. Electrochemical data and the amount of dye loading.

Dye	E_{0-0} [eV]	$E(S^+/S)$ [V][a]	$E(S^+/S^*)$ [V][a]	E_{gap} [V][b]	Dye loading [10^{-6} mol cm^{-2}]
4a[c]	2.84	0.87	−1.97	1.47	9.59
4b[c]	2.81	1.04	−1.77	1.27	2.79
32	2.81	0.69	−2.12	1.62	1.90

[a] Potentials are versus NHE. [b] Energy gap between the excited-state oxidation potential and TiO_2 conduction-band edge. [c] Data taken from ref. [12].

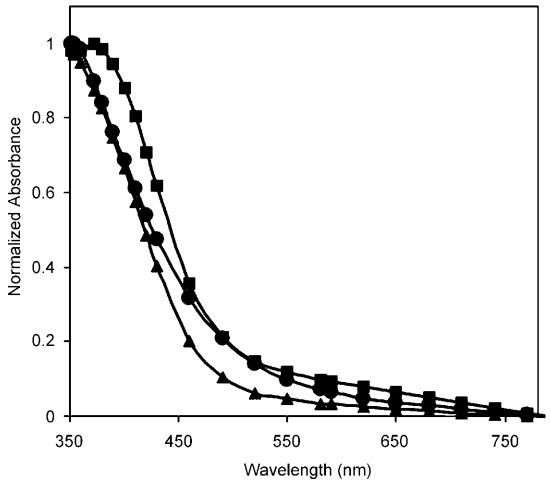

Figure 6. Normalized absorption spectra of dyes adsorbed on 1.5 μm TiO_2 films (●=**4a**, ■=**4b**, and ▲=**32**).

The oxidation potentials $E(S^+/S)$ of the dyes were measured by cyclic voltammetry (CV) and the results are collected in Table 4. To achieve efficient electron injection from the excited dye to the CB of the TiO_2, the energy level of the LUMO of the dye must be higher than the CB of the TiO_2 electrode. On the other hand, to achieve efficient regeneration of the oxidized state by electron transfer from I_3^-/I^- redox couple in the electrolyte, the energy level of the HOMO of the dye must be lower than the I_3^-/I^- redox potential. The oxidation potentials ranging from 0.69 to 1.04 V versus NHE are more positive than the redox mediator I^-/I_3^- ($\approx$0.4 V vs. NHE),[20] which ensures the efficient thermodynamic driving force (0.29–0.64 V) for dye regeneration. The excited-state oxidation potential $E(S^+/S^*)$ of these dyes can be obtained from the difference between the ground-state oxidation potential $E(S^+/S)$ and zero–zero excitation energy E_{0-0}, which was estimated from the cross section of the normalized absorption and emission spectra. As shown in Table 4, the excited-state oxidation potentials of the three dyes are more negative than the potential of the TiO_2 conduction-band edge (−0.5 V vs. NHE), which provides sufficient thermodynamic driving force (1.27–1.62 V) for electron injection.

Figure 7 illustrates the *J–V* curves and action spectrum of IPCE plots for the DSSCs based on the dyes studied in this work. The device performance of solar cells based on the

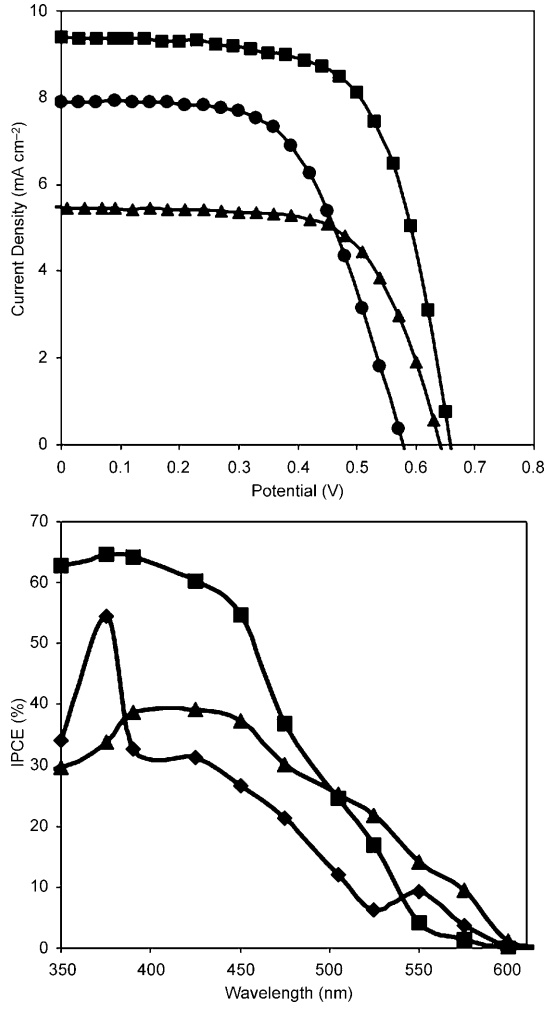

Figure 7.
J–V curves (top) and IPCE plots (bottom) of the dyes (●=**4a**, ■=**4b**, and ▲=**32**).

dyes is summarized in Table 5. The performance of the devices based on dyes **4b** reached up to 70% of the standard N719 dye. The photocurrent densities, J_{SC}, of the DSSCs are in the order of **4b** > **4a** > **32**, whereas the open circuit voltages, V_{OC}, are in the order of **4b** > **32** > **4a**. The reduced photovoltage observed in **4a** can be attributed to the less-bulky dimethylamino group in **4a** that is incapable of effectively blocking the infusion of the oxidized electrolyte I_3^- toward the TiO_2 surface and results in faster charge recombination between injected electron and oxidized electrolyte I_3^- when compared to the more bulky phenyindoline group in **32** and diphenylamino group in **4b**. The largest dark current generated from the DSSC based on **4a** among the three confirmed the fastest charge recombination in this case. This viewpoint is further supported by measuring the transient photovoltage decay at the open circuit.[21] Figure 8 shows the

Table 5. Photovoltaic performance parameters of the dyes.[a]

Dye	V_{OC} [mV]	J_{SC} [mA cm^{-2}]	*ff*	η [%][b]
4a[c]	577	7.89	0.59	2.69±0.20
4b[c]	660	9.40	0.65	4.03±0.01
32	641	5.44	0.67	2.34±0.08
N719[c]	695	11.9	0.71	5.87±0.02

[a] Experiments were performed using TiO_2 photoelectrodes with approximately 16 μm thickness and 0.25 cm^2 working area on the FTO (15 Ω per sq.) substrates with electrolyte composed of 0.05 M I_2, 0.5 M LiI, and 0.5 M *tert*-butylpyridine in acetonitrile solution under AM 1.5 illumination. [b] Average of three measurements. [c] Data taken from ref. [12].

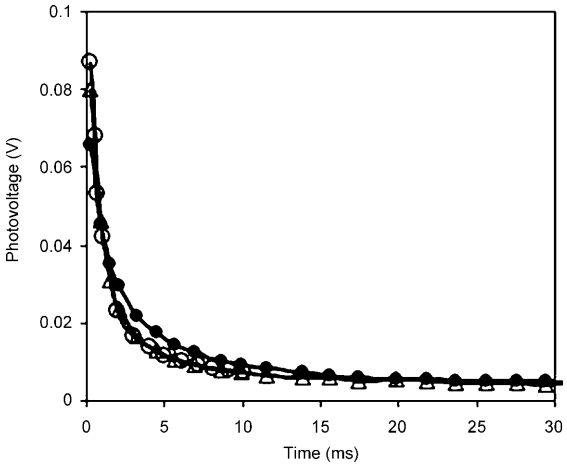

Figure 8. Traces of transient photovoltage decay of DSSCs based on dyes with 0.5 M LiI as the electrolyte in CH_3CN (△=**4a**, ●=**4b**, and ○=**32**).

transient photovoltage decay plots with LiI as the electrolyte. The electron lifetime was determined by fitting a decay of photovoltage transient with $\exp(-t/\tau)$, in which t is time and τ is an average time constant before recombination. The injected electron lifetimes obtained for **4a**, **4b**, and **32** are 2.93, 4.14, and 3.28 ms, respectively, which are in the order of **4b** > **32** > **4a** and in accordance with the observed order of V_{OC} shown in Table 5.

As shown in Tables 4 and 5, the amount of dye adsorbed onto the TiO_2 surface qualitatively correlated with the values of J_{SC}, with the lowest J_{SC} generated from the DSSC with the least amount of adsorbed dye. Beyond the better light-harvesting ability due to the higher surface-dye loading, it would be informative to correlate the photocurrent density to the accessibility of the TICT state of these dyes since the forbidden nature of radiative transition from a TICT state to the ground state is expected to slow down the charge recombination between the injected electron and photo-oxidized dye. To realize this argument, the electrochemical ac impedance of the cells was measured under the illumination conditions.[22] Figure 9 shows the electrochemical impedance Nyquist plots for DSSCs based on dyes **4a**, **4b**, and **32** measured under open-circuit conditions and under illumination of 100 mW cm^{-2}. The semicircle located in the midfrequency region is assigned to the charge transfer

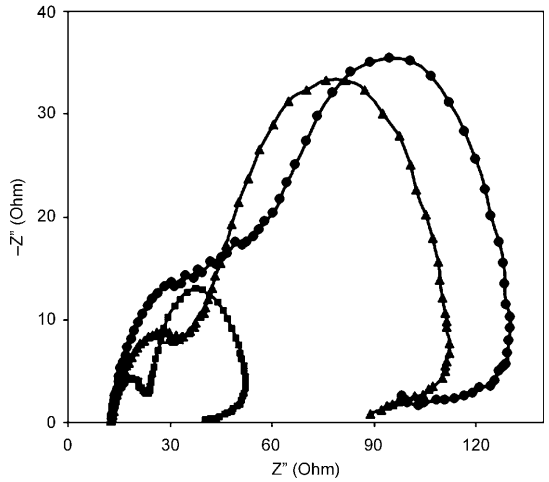

Figure 9. Electrochemical impedance Nyquist plots of DSSCs based on dyes measured under one sun illumination with open-circuit conditions (●=**4a**, ■=**4b**, and ▲=**32**).

at the TiO_2/dye/electrolyte interface.[23] The radius of the intermediate frequency semicircle of **4b** is much smaller than those of **4a** and **32**, thus indicating the much improved electron generation and transport in **4b** among the three dyes.[24] This result also corresponds well to that of the short-circuit current density shown in Table 5 in which the J_{SC} of **4b** is the highest among the three dyes.

Conclusion

In summary, a series of organic dyes that feature a 1,3-cyclohexadiene conjugated moiety integrated into the π-conjugated framework has been synthesized and studied. DSSCs based on these dyes have shown appreciable photo-to-electrical energy conversion efficiency with the highest one up to 4.03%. DSSCs based on the dye **4b**, which contain a diphenylamine moiety as the donor group, have better efficiency than DSSCs based on dyes **4a** and **32**. Dye **32** with a C–N bond, which fused to prevent the structural twisting between the phenylamino and benzene ring, served as a model compound for **4a** and **4b** to evaluate the related photophysical properties. Comprehensive photophysical studies and quantum calculations have suggested the accessibility of the TICT state for **4b** but not **4a** in polar solvents. The virtually forbidden nature of the radiative relaxation from the TICT state to the ground state renders DSSCs based on **4b** potent to resist the charge recombination between the photoinjected electron and the oxidized **4b**. The good correlation between the proposed TICT model and photocurrent generated from the DSSCs in our current work implies an useful guideline for designing highly efficient organic dyes for future progress of DSSCs. Our work on efficient dyes for DSSCs along this line is currently in progress.

Experimental Section

Materials and general procedures: The chemical 3-ethoxycyclohex-2-enone was synthesized according to the published method.[12] All other chemical reagents were commercially available and were used without further purification unless otherwise noted. Reactions were monitored by TLC using aluminum plates precoated with a 0.25 mm layer of silica gel that contained a fluorescent indicator.

Absorption spectra were obtained using a Perkin–Elmer Lambda 900 UV/Vis-NIR spectrophotometer or a Varian Cary 300 UV/Vis spectrophotometer. Emission spectra were recorded in an air-equilibrated solution using a Fluorolog III photoluminescence spectrometer.[25] Cyclic voltammetry experiments were performed using a CHI electrochemical analyzer. All measurements were carried out at room temperature with a conventional three-electrode configuration that consisted of a platinum working electrode, a platinum wire auxiliary electrode, and a nonaqueous $Ag/AgNO_3$ reference electrode. The potentials were quoted against the ferrocene internal standard. The solvent contained 1.0 mM of the dye and 0.1 M tetrabutylammonium hexafluorophosphate as supporting electrolyte in all experiments.

The photoelectrochemical characterizations on the solar cells were carried out using a modified light source, a 450 W Xe lamp (Oriel, 6266) equipped with a water-based IR filter and an AM 1.5 filter (Oriel, 81075). Light intensity, attenuated by neutral density filter (Optosigma, 078-0360) at the measuring (cell) position, was estimated to be around 100 mW cm^{-2} according to the reading from a radiant power meter (Oriel, 70260) connected to a thermopile probe (Oriel, 70263). Photocurrent/voltage curves of the DSSCs were recorded through the potentiostat/galvanostat (PGSTAT 30, Autolab, Eco-Chemie, Netherland).

Electrochemical impedance spectra were recorded for DSSCs under the same conditions at V_{OC} potential at room temperature. The frequencies explored ranged from 10 mHz to 65 kHz. The ac amplitude was set at 10 mV. The photovoltage transients of assembled devices were recorded using a digital oscilloscope (Tektronix, TDS 3012b). Pulsed laser excitation was applied by a Q-Switched Nd:YAG laser (Quanrel, brilliant B) with 10 Hz repetition rate at 532 nm and a 7 ns pulse width at half-height. The beam size was slightly larger than 0.25 cm^2 to cover the area of the device with incident energy of 3 mJ cm^{-2}. The recombination lifetime of injected electrons with oxidized dyes was measured by transient photovoltages at open circuit with the presence of LiI electrolyte (0.5 M). The average electron lifetime can be estimated approximately by fitting a decay of the open circuit voltage transient with $\exp(-t/\tau)$, in which t is time and τ is an average time constant before recombination.

Compound 29: *n*BuLi (2.5 M in *n*-hexane, 8.8 mL, 22 mmol) was added to a 250 mL flask charged with 5-bromo-1-phenylindoline (5.5 g, 20 mmol) and THF (100 mL) at −78 °C and stirred for 2 h. 3-Ethoxycyclohex-2-enone (2.5 g, 20 mmol) in THF (45 mL) was transferred to this mixture and the solution was stirred at −78 °C for 2 h. The reaction was quenched with aqueous NH_4Cl, extracted with ethyl acetate, dried with $MgSO_4$, and evaporated the solvent to afford the crude product. Column chromatography eluted with ethyl acetate/*n*-hexane (1:3) afforded compound **29** in 69% yield as a pale yellow solid. ^{1}H NMR (400 MHz, $CDCl_3$, 25 °C): δ=7.40–7.23 (m, 4H), 7.23 (d, ^3J(H,H)=7.7 Hz, 2H), 7.08 (d, ^3J(H,H)=8.5 Hz, 1H), 7.025 (t, ^3J(H,H)=7.7 Hz, 1H), 6.39 (s, 1H), 4.03 (t, ^3J(H,H)=8.5 Hz, 2H), 2.74 (t, ^3J(H,H)=6.1 Hz, 2H), 2.45 (t, ^3J(H,H)=7.3 Hz, 2H), 2.15–2.08 ppm (m, 2H); ^{13}C NMR (100 MHz, $CDCl_3$, 25 °C): δ=199.9, 159.4, 149.2, 143.1, 131.8, 129.3, 128.5, 126.3, 122.9, 122.10, 122.08, 118.3, 107.6, 52.4, 37.2, 27.8, 22.8 ppm; HRMS (EI): *m*/*z*: calcd for $C_{23}H_{23}NO_2$: 289.1467 [M^+]; found: 289.1467.

Compound 31: Compound **29** (1.04 g, 3.58 mmol) was dissolved in THF (45 mL) and the solution was cooled to −78 °C. The resulting mixture was transferred to a 100 mL flask that contained lithium diisopropylamide (LDA) prepared from diisopropylamine (4.65 mmol) and *n*-butyllithium (1.6 M solution in hexane, 3.0 mL, 4.8 mmol) at −78 °C for 45 min. Subsequently, ethyl chloroformate (0.6 mL, 5.37 mmol) was added to the reaction flask and stirred at −78 °C for another 45 min. The reaction was quenched with aqueous NH_4Cl, extracted with ethyl acetate, dried over

$MgSO_4$, and evaporated the solvent to afford the crude product. Flash column chromatography eluted with ethyl acetate/*n*-hexane (1:3) afforded ethyl 2-oxo-4-(1-phenylindolin-5-yl)cyclohex-3-enecarboxylate as a pale yellow solid. HRMS (EI): *m*/*z*: calcd: 361.1684 [M^+]; found: 361.1678.

$NaBH_4$ (0.29 g, 7.8 mmol) was added to a 100 mL flask charged with the ethyl 2-oxo-4-(1-phenylindolin-5-yl)cyclohex-3-enecarboxylate crude product (0.56 g, 1.6 mmol) and MeOH (50 mL) in an ice bath and the reaction progress was monitored by TLC. The reaction was quenched with aqueous NH_4Cl. After evaporating the volatile portion, the residue was extracted with ethyl acetate, dried over $MgSO_4$, and evaporated the solvent to afford the crude product. The crude product was redissolved in CH_2Cl_2 (50 mL) followed by addition of methanesulfonyl chloride (0.2 mL, 2.1 mmol) and NEt_3 (0.25 mL, 1.9 mmol) in the ice bath. The mixture was stirred at room temperature for 2.5 h. The reaction was quenched with aqueous NH_4Cl, extracted with CH_2Cl_2, dried over $MgSO_4$, and evaporated the solvent to afford the brownish residue. CH_2Cl_2 (50 mL) and 1,8-diazabicyclo[5.4.0]undec-7-ene (DBU; 0.3 mL, 2.1 mmol) were added to this residue in an ice bath and the mixture was stirred at room temperature for 8 h before being quenched with aqueous NH_4Cl. The residue was extracted with CH_2Cl_2, dried over $MgSO_4$, and evaporated the solvent to afford the crude product. Column chromatography eluted with ethyl acetate/*n*-hexane (1:30) afforded compound **31** in 39% yield as a dark yellow solid. ^{1}H NMR (500 MHz, $CDCl_3$, 25°C): δ = 7.35–7.32 (m, 3H), 7.25–7.20 (m, 4H), 7.16 (d, ^3J(H,H) = 6.0 Hz, 1H), 7.08 (d, ^3J(H,H) = 8.4 Hz, 1H), 6.98 (t, ^3J(H,H) = 7.3 Hz, 1H), 6.37 (d, ^3J(H,H) = 6.0 Hz, 1H), 4.22 (q, ^3J(H,H) = 7.1 Hz, 2H), 3.99 (t, ^3J(H,H) = 8.4 Hz, 2H), 3.13 (t, ^3J(H,H) = 8.4 Hz, 2H), 2.69–2.57 (m, 4H), 1.30 ppm (t, ^3J(H,H) = 7.1 Hz, 2H); ^{13}C NMR (125 MHz, $CDCl_3$, 25°C): δ = 167.6, 147.3, 143.6, 143.5, 134.6, 131.7, 130.4, 129.2, 125.0, 122.2, 121.5, 117.9, 117.1, 107.7, 60.2, 52.3, 27.9, 26.1, 22.0, 14.4 ppm; HRMS (EI): *m*/*z*: calcd for $C_{23}H_{23}NO_2$: 345.1729 [M^+]; found: 345.1738.

Compound 32: A 100 mL flask was charged with compound **31** (100 mg, 0.29 mmol), KOH (50 mg, 0.89 mmol), and MeOH/THF (50 mL, 5:1 in v/v) and the mixture was heated at reflux for 12 h. The volatile portion was removed under reduced pressure. The residue was neutralized to pH 7 with 1 M HCl. The aqueous solution was extracted with CH_2Cl_2 and dried over $MgSO_4$. Subsequent column chromatography eluted with ethyl acetate/*n*-hexane (1:1) afforded dye **32** in 53% yield as a pale orange solid. ^{1}H NMR (500 MHz, $CDCl_3$, 25°C): δ = 7.48 (s, 1H), 7.39–7.340 (m, 3H), 7.8 (d, ^3J(H,H) = 10.0 Hz, 2H), 7.18 (d, ^3J(H,H) = 5.0 Hz, 1H), 7.13 (d, ^3J(H,H) = 5.0 Hz, 1H), 6.99 (t, ^3J(H,H) = 5.0 Hz, 1H), 6.50 (d, ^3J(H,H) = 5.0 Hz, 1H), 4.03 (t, ^3J(H,H) = 10.0 Hz, 2H), 3.17 (t, ^3J(H,H) = 10.0 Hz, 2H), 2.70 (t, ^3J(H,H) = 10.0 Hz, 2H), 2.55 ppm (t, ^3J(H,H) = 10.0 Hz, 2H); ^{13}C NMR (125 MHz, $CDCl_3$, 25°C): δ = 168.3, 148.2, 144.6, 144.3, 135.4, 133.0, 130.4, 125.9, 125.2, 122.1, 118.6, 117.6, 111.4, 108.4, 52.9, 31.6, 26.5, 22.8 ppm; HRMS (EI): *m*/*z*: calcd for $C_{21}H_{19}NO_2$: 317.1416 [M^+]; found: 317.1420.

Acknowledgements

We thank the National Science Council in Taiwan, Academia Sinica, and the National Taiwan Normal University for support of this research.

[1] B. O'Regan, M. Grätzel, *Nature* **1991**, *353*, 737–740.

[2] a) M. K. Nazeeruddin, A. Kay, I. Rodicio, R. Humphry-Baker, E. Müller, P. Liska, N. Vlachopoulos, M. Grätzel, *J. Am. Chem. Soc.* **1993**, *115*, 6382–6390; b) M. K. Nazeeruddin, P. Péchy, T. Renouard, S. M. Zakeeruddin, R. Humphry-Baker, P. Comte, P. Liska, L. Cevey, E. Costa, V. Shklover, L. Spiccia, G. B. Deacon, C. A. Bignozzi, M. Grätzel, *J. Am. Chem. Soc.* **2001**, *123*, 1613–1624; c) M. Grätzel, *J. Photochem. Photobiol. A* **2004**, *164*, 3–14; d) C.-Y. Chen, J.-G. Chen, S.-J. Wu, J.-Y. Li, C.-G. Wu, K.-C. Ho, *Angew. Chem.* **2008**, *120*, 7452–7455; *Angew. Chem. Int. Ed.* **2008**, *47*, 7342–7345; e) C.-Y. Chen, S.-J. Wu, C.-G. Wu, J.-G. Chen, K.-C. Ho, *Angew. Chem.* **2006**, *118*, 5954–5957; *Angew. Chem. Int. Ed.* **2006**, *45*, 5822–5825; f) F. Gao, Y. Wang, D. Shi, J. Zhang, M. Wang, X. Jing, R. Humphry-Baker, P. Wang, S. M. Zakeeruddin, M. Grätzel, *J. Am. Chem. Soc.* **2008**, *130*, 10720–10728; g) B.-S. Chen, K. Chen, Y.-H. Hong, W.-H. Liu, T.-H. Li, C.-H. Lai, P.-T. Chou, Y. Chi, G.-H. Lee, *Chem. Commun.* **2009**, 5844–5846.

[3] a) S. Ito, S. M. Zakeeruddin, R. Humphry-Baker, P. Liska, R. Charvet, P. Comte, M. K. Nazeeruddin, P. Péchy, M. Takata, H. Miura, S. Uchida, M. Grätzel, *Adv. Mater.* **2006**, *18*, 1202–1205; b) T. Horiuchi, H. Miura, K. Sumioka, S. Uchida, *J. Am. Chem. Soc.* **2004**, *126*, 12218–12219; c) S. Hwang, J. H. Lee, C. Park, H. Lee, C. Kim, C. Park, M.-H. Lee, W. Lee, J. Park, K. Kim, N.-G. Park, C. Kim, *Chem. Commun.* **2007**, 4887–4889; d) S. Ito, H. Miura, S. Uchida, M. Takata, K. Sumioka, P. Liska, P. Comte, P. Péchy, M. Grätzel, *Chem. Commun.* **2008**, 5194–5196; e) G. Zhang, H. Bala, Y. Cheng, D. Shi, X. Lv, Q. Yu, P. Wang, *Chem. Commun.* **2009**, 2198–2200.

[4] a) R. Neil, *Angew. Chem.* **2006**, *118*, 2398–2405; *Angew. Chem. Int. Ed.* **2006**, *45*, 2338–2345; b) A. Mishra, M. K. R. Fischer, P. Bäuerle, *Angew. Chem.* **2009**, *121*, 2510–2536; *Angew. Chem. Int. Ed.* **2009**, *48*, 2474–2499.

[5] a) A. Hagfeldt, M. Grätzel, *Chem. Rev.* **1995**, *95*, 49–68; b) M. Grätzel, *Nature* **2001**, *414*, 338–344.

[6] a) A. Hagfeldt, M. Grätzel, *Acc. Chem. Res.* **2000**, *33*, 269–277; b) F. Matar, T. H. Ghaddar, K. Walley, T. DosSantos, J. R. Durrant, B. O'Regan, *J. Mater. Chem.* **2008**, *18*, 4246–4253; c) K. Chen, Y.-H. Hong, Y. Chi, W.-H. Liu, B.-S. Chen, P.-T. Chou, *J. Mater. Chem.* **2009**, *19*, 5329–5335; d) J.-F. Yin, D. Bhattacharya, Y.-C. Hsu, C.-C. Tsai, K.-L. Lu, H.-C. Lin, J.-G. Chen, K.-C. Ho, *J. Mater. Chem.* **2009**, *19*, 7036–7042.

[7] a) A. Abbotto, N. Manfredi, C. Marinzi, F. De Angelis, E. Mosconi, J.-H. Yum, Z. Xianxi, M. K. Nazeeruddin, M. Grätzel, *Energy Environ. Sci.* **2009**, *2*, 1094–1101; b) K. R. J. Thomas, Y.-C. Hsu, J. T. Lin, K.-M. Lee, K.-C. Ho, C.-H. Lai, Y.-M. Cheng, P.-T. Chou, *Chem. Mater.* **2008**, *20*, 1830–1840; c) Y.-S. Yen, Y.-C. Hsu, J. T. Lin, C.-W. Chang, C.-P. Hsu, D.-J. Yin, *J. Phys. Chem. C* **2008**, *112*, 12557–12567; d) J. T. Lin, P.-C. Chen, Y.-S. Yen, Y.-C. Hsu, H.-H. Chou, M.-C. P. Yeh, *Org. Lett.* **2009**, *11*, 97–100; e) S. Kim, J. K. Lee, S. O. Kang, J. Ko, J.-H. Yum, S. Fantacci, F. De Angelis, D. D. Censo, M. K. Nazeeruddin, M. Grätzel, *J. Am. Chem. Soc.* **2006**, *128*, 16701–16707; f) A. Abbotto, C. Barolo, L. Bellotto, F. de Angelis, M. Grätzel, N. Manfredi, C. Marinzi, S. Fantacci, J.-H. Yum, M. K. Nazeeruddin, *Chem. Commun.* **2008**, 5318–5320.

[8] a) Z. Ning, H. Tian, *Chem. Commun.* **2009**, 5483–5495 and references therein; b) H. Tian, X. Yang, J. Pan, R. Chen, M. Liu, Q. Zhang, A. Hagfeldt, L. Sun, *Adv. Funct. Mater.* **2008**, *18*, 3461–3468; c) G. Li, Y.-F. Zhou, X.-B. Cao, P. Bao, K.-J. Jiang, Y. Lin, L.-M. Yang, *Chem. Commun.* **2009**, 2201–2203.

[9] a) N. Hirata, J.-J. Lagref, E. J. Palomares, J. R. Durrant, M. K. Nazeeruddin, M. Grätzel, D. D. Censo, *Chem. Eur. J.* **2004**, *10*, 595–602; b) S. A. Haque, S. Handa, K. Peter, E. Palomares, M. Thelakkat, J. R. Durrant, *Angew. Chem.* **2005**, *117*, 5886–5890; *Angew. Chem. Int. Ed.* **2005**, *44*, 5740–5744.

[10] a) Z. R. Grabowski, K. Rotkiewicz, W. Rettig, *Chem. Rev.* **2003**, *103*, 3899–4031 and references therein; b) R. Chen, G. Zhao, X. Yang, X. Jiang, J. Liu, H. Tian, Y. Gao, X. Liu, K. Han, M. Sun, L. Sun, *J. Mol. Struct.* **2008**, *876*, 102–109.

[11] a) E. Lippert, W. Rettig, V. Bonacic-Koutecky, F. Heisel, J. A. Miehe, *Adv. Chem. Phys.* **1987**, *68*, 1–174; b) J.-S. Yang, K.-L. Liau, C.-Y. Li, M.-Y. Chen, *J. Am. Chem. Soc.* **2007**, *129*, 13183–13192; c) S. S. Palayangoda, X. C. Cai, R. M. Adhikari, D. C. Neckers, *Org. Lett.* **2008**, *10*, 281–284; d) M. S. Yuan, Z. Q. Liu, Q. Fang, *J. Org. Chem.* **2007**, *72*, 7915–7922; e) S. Cogan, S. Zilberg, Y. Haas, *J. Am. Chem. Soc.* **2006**, *128*, 3335–3345; f) E. Lippert, W. Lüder, F. Moll, W. Nägele, H. Boos, H. Prigge, I. Seibold-Blankenstein, *Angew. Chem.* **1961**, *73*, 695–706; g) L. Serrano-Andrés, M. Merchán, B. O. Roos, R. Lindh, *J. Am. Chem. Soc.* **1995**, *117*, 3189–3204; h) W. Rettig, *Angew. Chem.* **1986**, *98*, 969–986; *Angew. Chem. Int. Ed. Engl.* **1986**, *25*, 971–988; i) C. Jamorski Jödicke, H. P. Löthi, *J. Am. Chem. Soc.* **2003**, *125*, 252–264; j) D. Rappoport, F. Furche, *J. Am.*

Chem. Soc. **2004**, *126*, 1277–1284; k) I. Gómez, M. Reguero, M. Boggio-Pasqua, M. A. Robb, *J. Am. Chem. Soc.* **2005**, *127*, 7119–7129; l) U. Resch-Genger, Y. Q. Li, J. L. Bricks, V. Kharlanov, W. Rettig, *J. Phys. Chem. A* **2006**, *110*, 10956–10971; m) R. Hu, E. Lager, A. Aguilar-Aguilar, J. Liu, J. W. Y. Lam, H. H. Y. Sung, I. D. Williams, Y. Zhong, K. S. Wong, E. Peña-Cabrera, B. Z. Tang, *J. Phys. Chem. C* **2009**, *113*, 15845–15853; n) G.-J. Zhao, R.-K. Chen, M.-T. Sun, J.-Y. Liu, G.-Y. Li, Y.-L. Gao, K.-L. Han, X.-C. Yang, L. Sun, *Chem. Eur. J.* **2008**, *14*, 6935–6947; o) J.-S. Yang, C.-K. Lin, A. M. Lahoti, C.-K. Tseng, Y.-H. Liu, G.-H. Lee, S.-M. Peng, *J. Phys. Chem. A* **2009**, *113*, 4868–4877.

[12] K.-F. Chen, Y.-C. Hsu, Q.-Y. Wu, M.-C. P. Yeh, S.-S. Sun, *Org. Lett.* **2009**, *11*, 377–380.

[13] J.-S. Yang, K.-L. Liau, C.-M. Wang, C.-Y. Hwang, *J. Am. Chem. Soc.* **2004**, *126*, 12325–12335.

[14] T.-P. Lin, C.-Y. Chen, Y-S. Wen, S.-S. Sun, *Inorg. Chem.* **2007**, *46*, 9201–9212.

[15] W. Baumann, H. Bischof, J.-C. Frhling, C. Brittinger, W. Rettig, K. Rotkiewicz, *J. Photochem. Photobiol. A* **1992**, *64*, 49–72.

[16] a) J. Saltiel, A. Marinari, D. W.-L. Chang, J. C. Mitchener, E. D. Megarity, *J. Am. Chem. Soc.* **1979**, *101*, 2982–2996; b) J.-S. Yang, S.-Y. Chiou, K.-L. Liau, *J. Am. Chem. Soc.* **2002**, *124*, 2518–2527.

[17] Z.-S Wang, K. Hara, Y. Dan-oh, C. Kasada, A. Shinpo, S. Suga, H. Arakawa, H. Sugihara, *J. Phys. Chem. B* **2005**, *109*, 3907–3914.

[18] a) W. Xu, B. Peng, J. Chen, M. Liang, F. Cai, *J. Phys. Chem. C* **2008**, *112*, 874–880; b) Z. Ning, Q. Zhang, W. Wu, H. Pei, B. Liu, H. Tian, *J. Org. Chem.* **2008**, *73*, 3791–3797; c) Z.-S. Wang, N. Koumura, Y. Cui, M. Takahashi, H. Sekiguchi, A. Mori, T. Kubo, A. Furube, K. Hara, *Chem. Mater.* **2008**, *20*, 3993–4003; d) Y. Ooyama, A. Ishii, Y. Kagawa, I. Imae, Y. Harima, *New J. Chem.* **2007**, *31*, 2076–2082.

[19] J. R. Mann, M. K. Gannon, T. C. Fitzgibbons, M. R. Detty, D. F. Watson, *J. Phys. Chem. C* **2008**, *112*, 13057–13061.

[20] N. Koumura, Z.-S. Wang, S. Mori, M. Miyashita, E. Suzuki, K. Hara, *J. Am. Chem. Soc.* **2006**, *128*, 14256–14257.

[21] N. Kopidakis, K. D. Benkstein, J. van de Lagemaat, A. J. Frank, *J. Phys. Chem. B* **2003**, *107*, 11307–11315.

[22] a) J. van de Lagemaat, N.-G. Park, A. J. Frank, *J. Phys. Chem. B* **2000**, *104*, 2044–2052; b) Q. Wang, J.-E. Moser, M. Grätzel, *J. Phys. Chem. B* **2005**, *109*, 14945–14953; c) D. Kuang, S. Ito, B. Wenger, C. Klein, J.-E. Moser, R. Humphry-Baker, S. M. Zakeeruddin, M. Grätzel, *J. Am. Chem. Soc.* **2006**, *128*, 4146–4154.

[23] a) C. Longo, A. F. Nogueira, M.-A. de Paoli, H. Cachet, *J. Phys. Chem. B* **2002**, *106*, 5925–5930; b) R. Kern, R. Sastrawan, J. Ferber, R. Stangl, J. Luther, *Electrochim. Acta* **2002**, *47*, 4213–4225.

[24] a) H. Choi, S. Kim, S. O. Kang, J. Ko, M.-S. Kang, J. N. Clifford, A. Forneli, E. Palomares, M. K. Nazeeruddin, M. Grätzel, *Angew. Chem.* **2008**, *120*, 8383–8387; *Angew. Chem. Int. Ed.* **2008**, *47*, 8259–8263; b) J.-J. Kim, H. Choi, J.-W. Lee, M.-S. Kang, K. Song, S. O. Kang, J. Ko, *J. Mater. Chem.* **2008**, *18*, 5223–5229.

[25] a) C.-Y. Wu, M.-S. Chen, C.-A. Lin, S.-C. Lin, S.-S. Sun, *Chem. Eur. J.* **2006**, *12*, 2263–2269; b) C.-L. Chen, T.-P. Lin, Y.-S. Chen, S.-S. Sun, *Eur. J. Org. Chem.* **2007**, 3999–4010.

Received: May 13, 2010
Published online: September 30, 2010

